

S1. Experimental section

S1.1. Materials required

Ferric chloride hexahydrate ($\text{FeCl}_3 \cdot 6\text{H}_2\text{O}$, MW: 270.3 g/mol), Terephthalic acid ($\text{C}_6\text{H}_4(\text{COOH})_2$, MW: 166.13 g/mol), Cobalt chloride hexahydrate ($\text{CoCl}_2 \cdot 6\text{H}_2\text{O}$, MW: 237.93 g/mol), Sodium peroxydisulfate ($\text{Na}_2\text{S}_2\text{O}_8$, PDS, MW: 298.03 g/mol), Oxone (Potassium peroxymonosulfate, PMS, 2KHSO_5 , KHSO_4 , K_2SO_4 , MW: 307.38 g/mol), Triethyl amine (TEA, $(\text{C}_2\text{H}_5)_3\text{N}$, MW: 101.19 g/mol), Tert-butyl alcohol (TBA, $(\text{CH}_3)_3\text{COH}$, MW: 74.12 g/mol), L-histidine (His, MW: 155.56 g/mol), p-Benzoquinone (pBQ, MW: 108.09 g/mol), Sodium chloride (NaCl , MW: 58.5 g/mol), Sodium sulfate (Na_2SO_4 , MW: 142.04 g/mol), Sodium nitrate (NaNO_3 , MW: 85 g/mol), Sodium carbonate (Na_2CO_3 , MW: 106 g/mol), Disodium hydrogen phosphate (Na_2HPO_4 , MW: 142 g/mol), Humic acid (HA, 60-70% dry basis), sodium perchlorate monohydrate ($\text{NaClO}_4 \cdot \text{H}_2\text{O}$, MW: 140.46 g/mol), sodium azide (NaN_3 , MW: 65.01 g/mol), L-Ascorbic acid ($\text{C}_6\text{H}_8\text{O}_6$, MW: 176.12 g/mol), furfuryl alcohol ($\text{C}_5\text{H}_6\text{O}_2$, MW: 98.1 g/mol), potassium iodide (KI, MW: 166.0 g/mol), Rhodamine B (RhB, $\text{C}_{28}\text{H}_{31}\text{ClN}_2\text{O}_3$) were purchased from M/s. Loba Chemie Pvt. Ltd., India. Methanol (CH_3OH , MW: 32.04 g/mol) was obtained from M/s. Spectrochem Pvt. Ltd., Mumbai, India. Dimethyl sulphoxide (DMSO, $\text{C}_2\text{H}_6\text{OS}$, MW: 78.13 g/mol), Ethylene diamine tetraacetic acid disodium salt (EDTA-2Na, MW: 372.24 g/mol) and N,N-dimethyl formamide (DMF, MW: 73.09 g/mol) were procured from M/s. Merck Life sciences Pvt. Ltd., India. 5,5-Dimethyl-1-pyrroline N-oxide (DMPO, $\text{C}_6\text{H}_{11}\text{NO}$, MW: 113.16 g/mol), 2,2,6,6-Tetramethylpiperidine 1-oxyl, 2,2,6,6-Tetramethyl-1-piperidinyloxy (TEMPO, $\text{C}_9\text{H}_{18}\text{NO}$, MW: 156.25 g/mol), Titanium isopropoxide ($\text{Ti}[\text{OCH}(\text{CH}_3)_2]_4$, MW: 284.22 g/mol, 97%), 2-Amino Terephthalic acid ($\text{H}_2\text{NC}_6\text{H}_3-1,4-(\text{COOH})_2$, MW: 181.15 g/mol, 99%), Tetracycline (TC, $\text{C}_{22}\text{H}_{24}\text{N}_2\text{O}_8$, analytical standard, purity $\geq 99\%$) and Carbamazepine (CBZ, $\text{C}_{15}\text{H}_{12}\text{N}_2\text{O}$, analytical standard, $\geq 98\%$, MW: 236.27 g/mol) were purchased from Sigma-Aldrich, USA. Deionized (DI) water (resistivity: 18.2 $\text{M}\Omega\cdot\text{cm}$) used in this study was obtained from a Millipore water purification system supplied by Merck (India) Pvt. Ltd. All the chemicals were of analytical grade and used without any further purification. All glassware used in this study were procured from Borosil glass works Pvt. Ltd., Kolkata, India.

S1.2. Synthesis of materials

The MIL-53(Fe/Co) MOF was developed using a previously described process ¹. In a typical synthesis method, 70 ml of DMF was added to a 100 ml capacity teflon cup. Then, 0.28 g of CoCl₂, 6H₂O, and 0.27 g of FeCl₃, 6H₂O were added while the mixture was constantly stirred. After these salts had completely dissolved, 1 g of terephthalic acid was added to the mixture. The mixture was allowed to homogenize for a further hour. The apparatus was then filled with a 5 ml DI water and 5 ml ethanol mixture. The teflon cup was placed within stainless steel autoclave reactor, and assembly was heated at 130°C for 12 hours at a rate of 1.1°C/min. After the reaction was completed, the mixture was allowed to cool naturally to ambient temperature. The suspension was centrifuged many times and repeatedly cleaned with DI water and ethanol before being recovered as a light brown solid. To produce the MOF powder, the material was cleaned, and then dried overnight in a vacuum at 85°C. For the NH₂-MIL-53(Fe/Co) MOF, similar hydrothermal procedure was followed, except 1.09 g of amino-terephthalic acid (NH₂-bdc) was added in place of terephthalic acid as the organic linker. The produced dark brown MOF was thoroughly cleaned using DI water and ethanol before being dried at 85°C in a hot air oven.

The MOF MIL-125(Ti) was created in accordance with a previously reported methodology ²⁻⁴. Briefly, 1.03 g of terephthalic acid (bdc) was continuously stirred into a mixture of 72 ml methanol and 8 ml dimethyl formamide (DMF). 1.2 ml of Ti-isopropoxide was added dropwise after full dissolution, with immediate formation of white solid dispersion. The mixture was stirred for another 30 mins and subsequently transferred in a teflon cup of 100 ml capacity. The assembly was heated for 24 h at 150°C with the cup enclosed in a stainless-steel autoclave reactor. The assembly was allowed to cool naturally once the reaction was finished. Centrifugation and vigorous washing with ethanol and DI water were used to separate the white powder. For future investigations, the cleaned material was stored in opaque glass vials, after being dried at 85° to 90°C in a hot air oven. For the NH₂-MIL-125(Ti) MOF, similar synthesis protocol was used. Here, in place of Terephthalic acid, amino-terephthalic acid (NH₂-bdc) was employed. A mixture of 1.12 g of NH₂-bdc and 1.2 ml of Ti-isopropoxide was dissolved in a mixture of 72 ml methanol and 8 ml DMF and the resultant mixture was hydrothermally treated at 150°C for 24 h. Bright yellow NH₂-MIL-125(Ti) crystals were produced and further collected through multiple washing and drying at 85°C in a hot air oven.

S1.3. Characterization methods

The synthesized materials (MIL-125(Ti), MIL-53(Fe/Co), NH₂-MIL-125(Ti), NH₂-MIL-53(Fe/Co) and binary composites) were characterized by different techniques. The crystal microstructure and surface morphology of the materials were observed using a field emission scanning electron microscope (FESEM, model: JSM-7650F, JEOL, Japan). Crystallographic structure of the materials was studied using X-ray diffraction technique (XRD, model: Panalytical Xpro, Panalytical, The Netherlands) using Cu-K α radiation ($\lambda = 1.5418 \text{ \AA}$) within scanning range of 7.5° to 85°. Surface functionalization and chemical bonding of the materials were determined using Fourier transform infrared spectroscopy (FTIR, model: Analyst 100, Perkin Elmer, The Netherlands). Oxidation states of the elements in the samples were studied using X-ray photoelectron spectroscopy (XPS, model: PHI 5000 VERSAPROBE– II M/S. Physical Electronics, USA). The same instrument was employed to carry out the valence band (VB) XPS analysis of the primary components. Porous structure (pore radius, pore volume, etc.) of the solid materials was determined through N₂ adsorption-desorption technique using a BET analyzer (model: Autosorb 1, Quantachrome Instruments, UK). Zeta potential of the material in aqueous solution was determined using a zetasizer (model: zetasizer nano, Malvern Instruments, USA). Diffuse reflectance UV-Vis absorption spectra of the catalysts were captured with a UV-Vis spectrophotometer (model: Cray 5000, Agilent Technologies, USA) using BaSO₄ as the reflectance standard reference. The obtained data was then converted to absorbance by the Kubelka-Munk method. The photoluminescence spectra (PL) were obtained with a spectrometer (HORIBA scientific, model: TRIAX 320- SAQIII- Vis (photon), USA). The validation of reactive oxidative species was performed with an Electron paramagnetic resonance spectrometer (EPR, X-band, Bruker, model: ELEXSYS 580) with the magnetic field scan range ± 2 Tesla. The photo electrochemical (PEC) measurements were carried out in a CHI 760D electrochemical workstation (CHI instruments, USA) using a three-electrode configuration (ITO glass substrate, Pt wire and Ag/AgCl reference electrode) in presence of 0.5(M) Na₂SO₄ electrolyte and 300 W Xenon arc lamp as irradiation source. The electron impedance spectroscopy (EIS) and Mott-Schottky analysis were carried out in the frequency domain of 1 Hz- 100 Hz and 5mV arc voltage amplitude.

S1.4. Experimental procedure

All the catalytic degradation experiments were carried out using Erlenmeyer flasks of 250 ml capacity, under constant rotation and visible light irradiation, unless otherwise specified. Stock

solution of CBZ was prepared by dissolving specified amount of CBZ powder in measured amount of DI water, under constant stirring. The final solution had concentration of 100 mg/L CBZ and was further kept at 4°C, for minimum concentration variation. The stock solution was suitably diluted using DI water to prepare solutions having lower concentrations. In a typical experiment, 50 ml CBZ solution having concentration of 10 mg/L was taken in number of flasks and specified amount of catalyst powder was added into the solution. The resultant mixtures were maintained under constant stirring at 150 rpm for 0.5 h, in absence of any visible light irradiation, to allow the establishment of adsorption-desorption equilibrium. Then, suitable dose of PMS was added into the suspension and visible light irradiation was turned on to initiate the photocatalytic reaction. For kinetic experiments, particular flask was withdrawn at specified predetermined time and the sample was collected through filtration using 0.45 µm PTFE filters to separate the solid powder from the liquid. The collected samples were immediately quenched using 1 ml 0.1(M) sodium thiosulfate solution and were further maintained at 4°C until analyzed, to determine the residual concentration of CBZ in the medium. This data was plotted as a function of reaction time to determine the profile of variation of residual amount of CBZ in the system and the rate of the degradation reaction. For other control experiments, kinetic studies were performed at different temperatures. Further, variation of different parameters, i.e., catalyst dose, PMS dose, initial concentration of CBZ, solution pH, process temperature, effects of coexisting ions and organics, etc., were carried out, maintaining other operational parameters invariant. Solution pH was tuned using either 0.1(M) HCl or 0.1(M) NaOH, as required. Radical scavenging experiments were performed in presence of different radical scavengers, through kinetic studies. EPR analysis was carried out, in presence of DMPO and TEMPO as spin-trapping agents, to determine the relative abundances of various radicals. No buffer solution was used to maintain the solution pH at the initial values. To determine the reusability and stability of the catalyst, the solid powder was collected after each experiment, washed thoroughly with DI water and ethanol, dried at 85°C in vacuum and used for further experiments. The variation of catalytic efficiency after each experiment was used as the measure of reusability of the material (in terms of performance). Finally, all the experiments were performed in triplicate and the mean values, along with the standard deviations were reported. The catalytic degradation of CBZ was modeled using pseudo first order kinetic model represented as: $-\ln\left(\frac{C}{C_0}\right) = k_{obs}t$, where, k_{obs} is the kinetic rate constant,

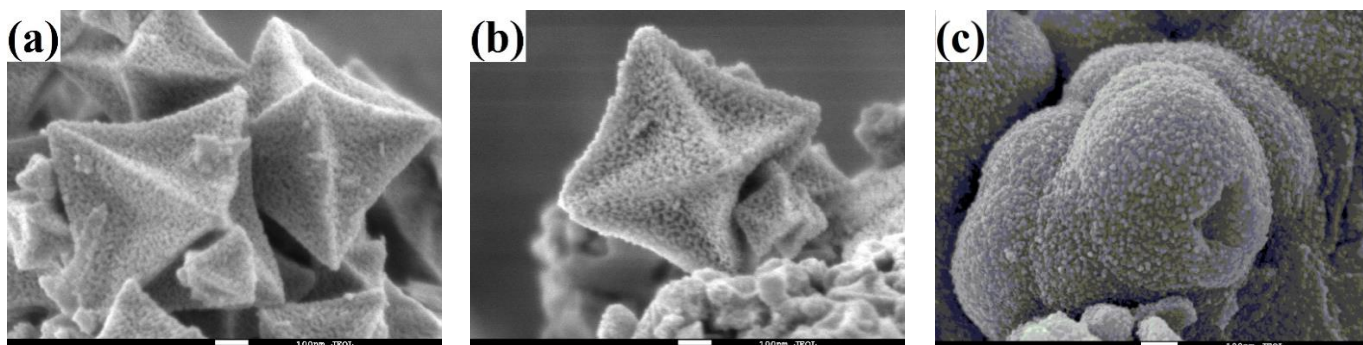
t is the treatment time, C and C_0 are the temporal CBZ concentration and feed concentration, respectively.

With RhB and TC, similar degradation experiments were conducted with optimized doses of catalyst and PMS, in presence of visible light. The residual concentration of RhB and TC were measured using an UV-Vis spectrophotometer (model: Lambda 35, Perkin Elmer, USA) at characteristic wavelengths of maximum absorbance of 554 nm and 357 nm, respectively.

S1.5. Analytical procedure

The residual concentration of CBZ in solution was determined using a high-performance liquid chromatography system (HPLC, model: series 200 UV-Vis system, Perkin Elmer, USA) with reversed phase Agilent SB C-18 column and a Perkin Elmer series 200 UV-Vis detector set at 284 nm. The mobile phase consisted of acetonitrile of HPLC grade (phase A) and ultrapure water (phase B) at 30:70 volume ratio at flowrate of 1 ml/min and column temperature was maintained at 30°C. Solution pH was measured using a pH meter (model: PCSTestr 35, Eutech instruments, Singapore). The intermediate analysis study was carried out based on a molecular mass distribution spectra determined using MALDI-TOFMS instrument (model: Ultraflex extreme, Bruker Daltonik GmbH Life Sciences, Germany). The total organic carbon (TOC) of the solution was measured using a TOC analyzer (model: TOC-L, Shimadzu corporation, Japan). Concentration of leached heavy metals (Fe, Co) was measured using an inductively coupled plasma emission spectroscopy-mass spectrometry instrument (ICP MS, model: iCAP™ RQ, Thermo-Fisher Scientific, USA) and atomic absorption spectroscopy (AAS, model: Analyst-700 coupled with MHS-15, Perkin Elmer Instruments, USA).

S1.6. Results and discussion



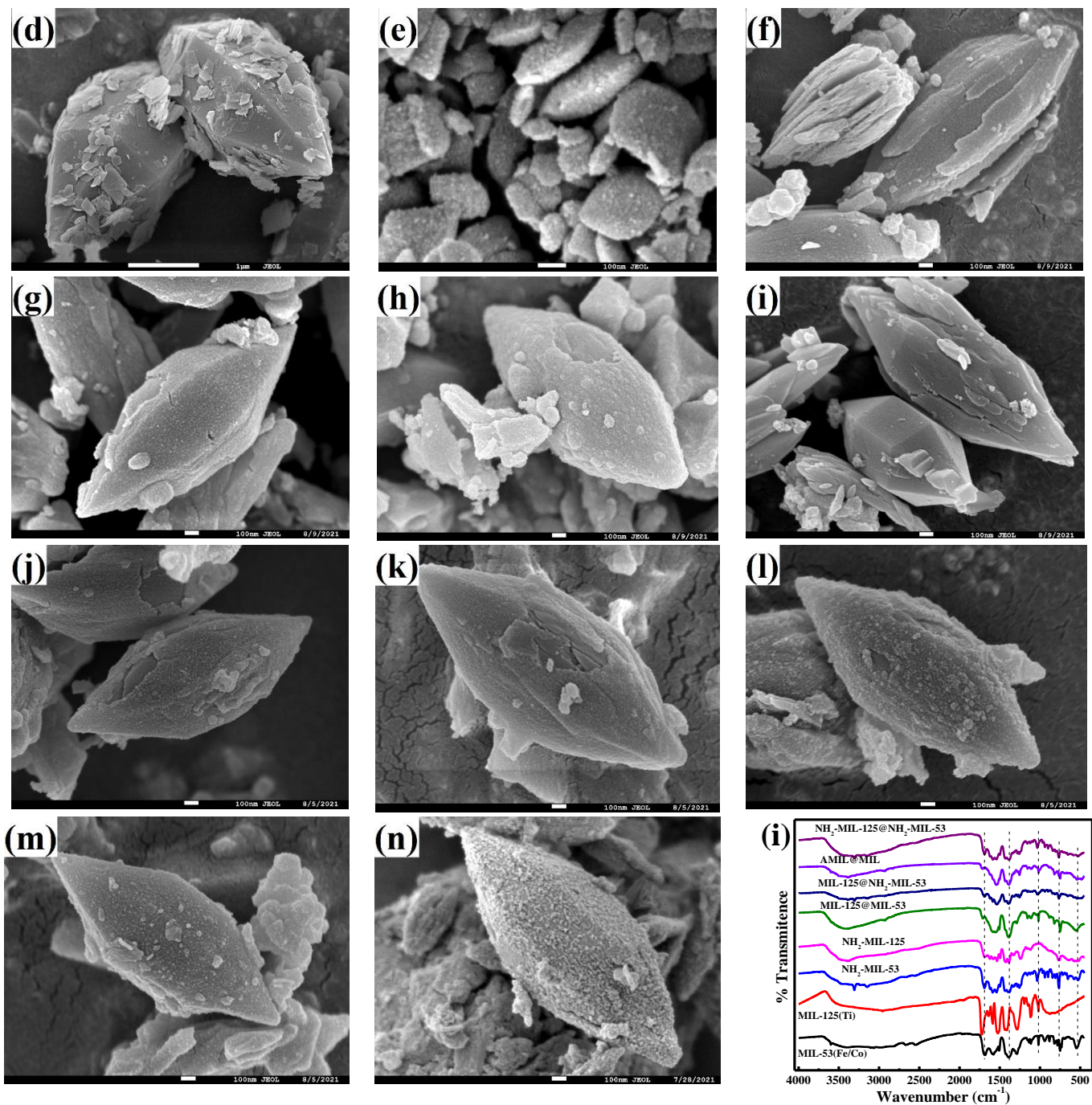
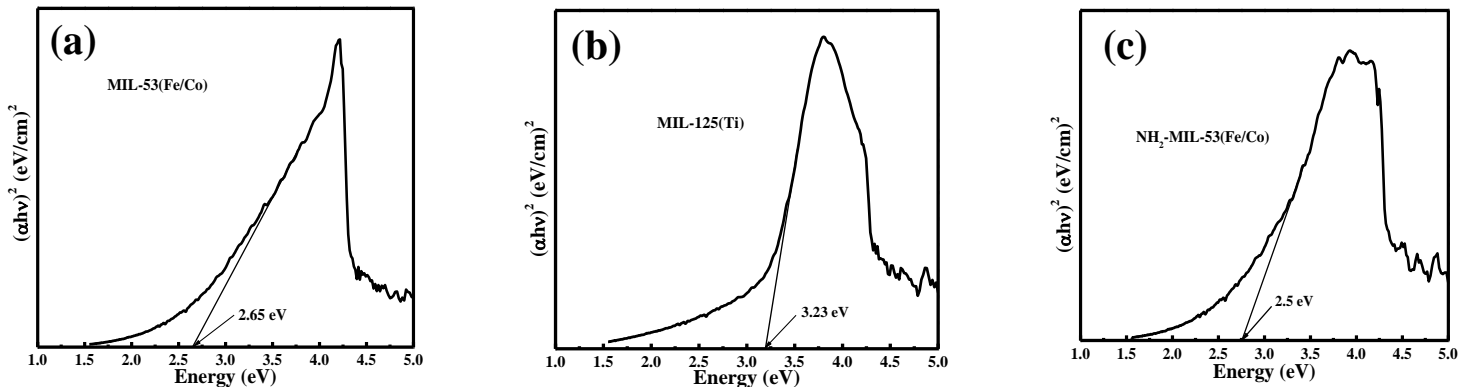


Fig. S1. FESEM images of (a,b) nascent MIL-53(Fe/Co); (c) nascent MIL-125(Ti); (d) nascent NH₂-MIL-53(Fe/Co); (e) nascent NH₂-MIL-125(Ti); (f-n) intermittent NH₂-MIL-125(Ti)@MIL-53(Fe/Co); (i) FTIR spectra of all primary MOFs and binary composites.

S1.6.1. FTIR analysis

In the FTIR spectrum of pure MIL-53 (Fig. S1i), the symmetric and asymmetric vibrations of the C-O and the C=O stretching of the -COOH groups yield three peaks at 1385 cm^{-1} , 1577 cm^{-1} , and 1689 cm^{-1} , respectively. The benzene rings of terephthalic acid linkers involve C-H bending with a peak at 699 cm^{-1} . Two small peaks are observed at 579 cm^{-1} and 481 cm^{-1} , due to the vibrations of Co-O and Fe-O bonding in the metal-terephthalic acid linkages. For nascent NH_2 -MIL-125(Ti), absorption bands due to $\nu(\text{C}=\text{C})$ skeletal vibrations of benzene rings are observed at 1536 cm^{-1} and 1424 cm^{-1} , respectively. Similarly, the C-H in-plane and out of plane bending vibrations generate peaks at 1264 cm^{-1} and 1160 cm^{-1} , respectively. Also, three small to medium peaks at 540 cm^{-1} , 648 cm^{-1} and 767 cm^{-1} are indicative of the O-Ti-O bonding in the composite. On the other hand, for pure MIL-125(Ti), the characteristic peaks due to O-Ti-O bonds are generated at 552 cm^{-1} , 631 cm^{-1} and 735 cm^{-1} , along with peaks due to aromatic C=C vibrations at 1411 cm^{-1} , 1437 cm^{-1} and 1520 cm^{-1} . The C-H in-plane and out of plane bending vibrations generate peaks at 1281 cm^{-1} and 1145 cm^{-1} . The overall broad flat absorption band within the 2900-3600 cm^{-1} are due to the -OH and -NH stretching vibrations. In comparison, for the NH_2 -MIL-53 spectrum, different peaks from -NH, C=C and aromatic ring vibrations are generated in the 1035-1688 cm^{-1} range. The Fe-O and Co-O bond vibrations generate two short but distinct peaks at 525 cm^{-1} and 580 cm^{-1} . Any of the binary composites contains features of all the primary components. As an example, for AMIL(10)@MIL composite, peaks due to the Fe-O (479 cm^{-1}), Co-O (542 cm^{-1}) and O-Ti-O (585 cm^{-1} , 656 cm^{-1} and 749 cm^{-1}) bonds can be identified, along with the strong presence of surface-anchored -NH₂ groups (at 1155 cm^{-1} , 1254 cm^{-1} , 1434 cm^{-1} and 1544 cm^{-1}). Also, the broad peak within the 3050-3470 cm^{-1} range, with a sharp peak at 3386 cm^{-1} is indicative of strong presence of surface-bound -OH and -NH groups. This study also indicates the successful formation of the binary AMIL@MIL composites.



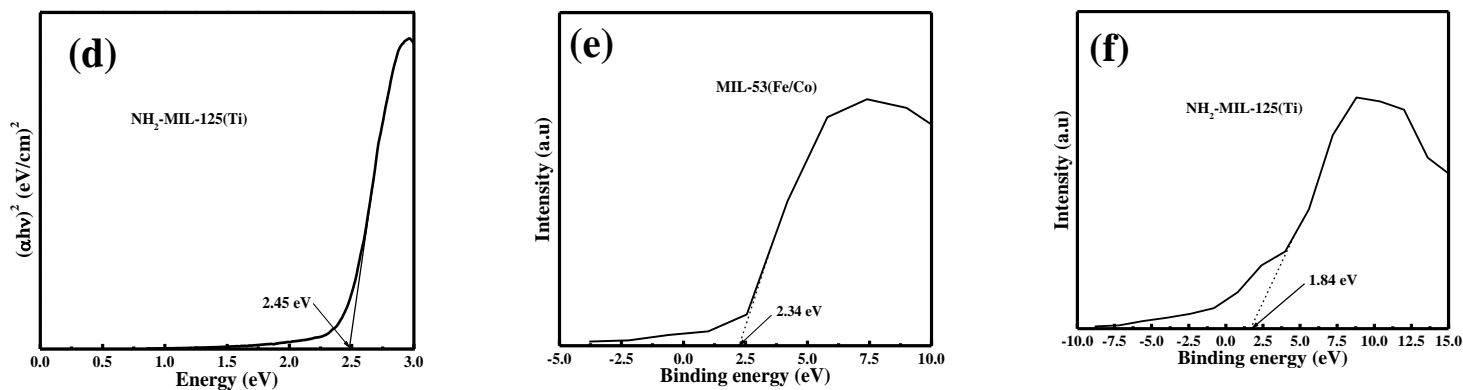
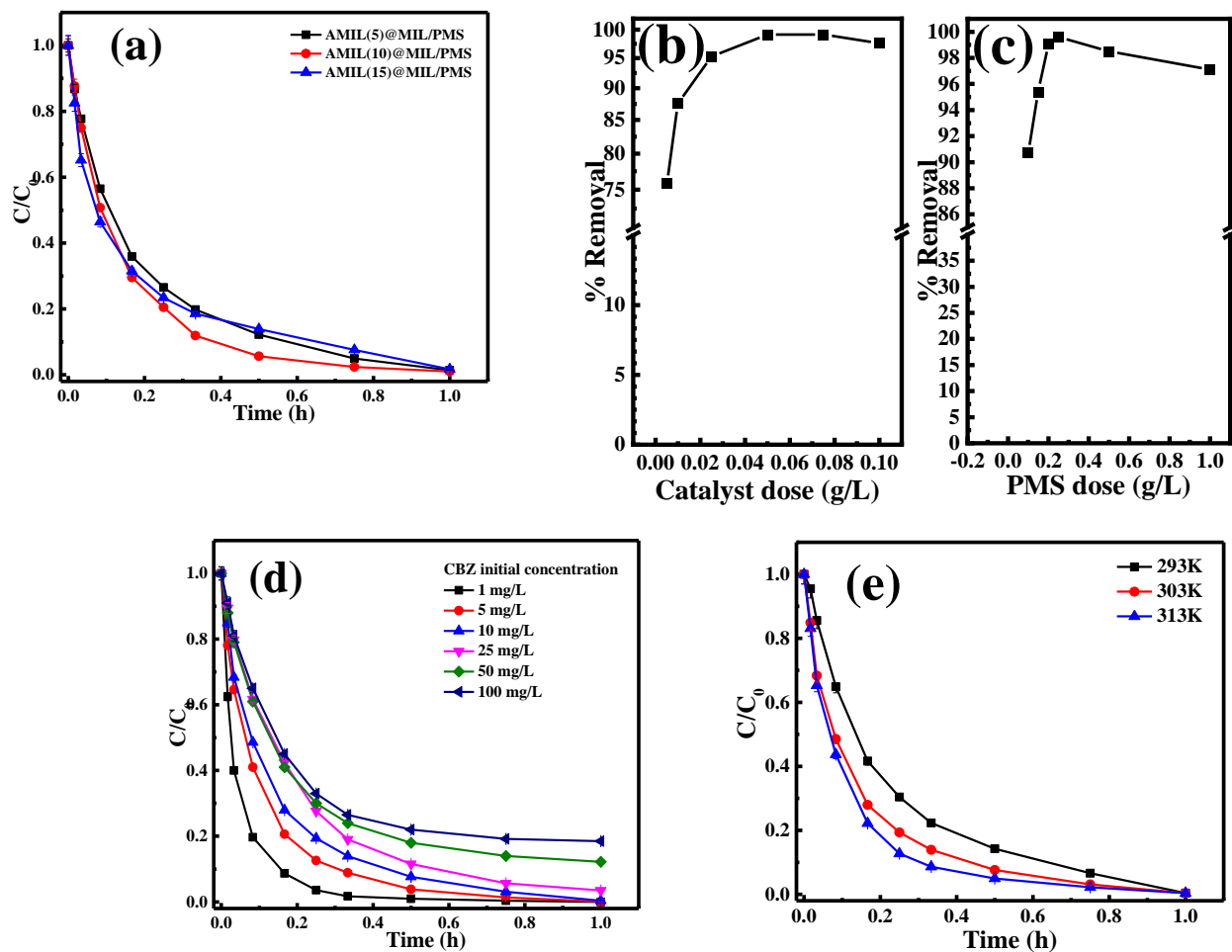


Fig. S2. Tauc's plot for (a) MIL-53(Fe/Co); (b) MIL-125(Ti); (c) NH₂-MIL-53(Fe/Co); (d) NH₂-MIL-125(Ti); VB XPS spectra for (e) MIL-53(Fe/Co); (f) NH₂-MIL-125(Ti).



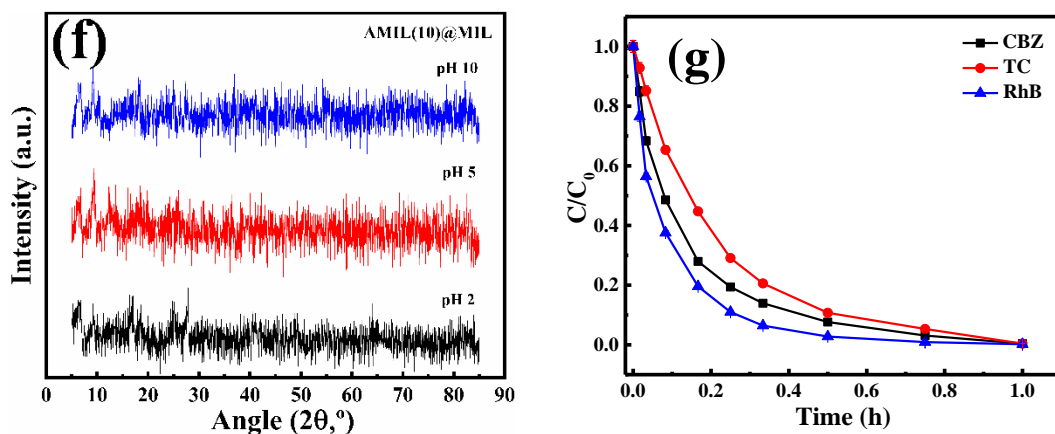


Fig. S3. Variation of residual CBZ concentration for (a) different AMIL@MIL composites; (b) variation of catalyst dose; (c) variation of PMS dose; (d) different initial CBZ concentration; (e) different operating temperatures; (f) XRD analysis of AMIL(10)@MIL at different operational pHs; (g) comparative degradation of different emerging contaminants, (experimental conditions: catalyst dose: 0.05 g/L (except for Fig. S3b), PMS dose: 0.25 g/L (except Fig. S3c), CBZ initial concentration: 10 mg/L (except Fig. S3d), TC initial concentration: 25 mg/L, RhB initial concentration: 100 mg/L, initial solution pH: 6.5, operating temperature: 30°C (except Fig. S3e).

S2. EPR analysis

Similar observations were obtained from the EPR analysis. As shown in Figs. S4(a,b), the DMPO- $\cdot\text{OH}$ and DMPO- $\text{SO}_4^{\bullet-}$ adducts generate the characteristic quartet (intensity ratio = 1:2:2:1) and sextet (intensity ratio = 1:1:1:1:1:1) patterns, having gradually increasing intensity with duration of visible light irradiation, implying generation of abundant $\cdot\text{OH}$ and $\text{SO}_4^{\bullet-}$ in the medium, respectively, along with characteristic quartet peaks (intensity ratio = 1:1:1:1) of DMPO- $\text{O}_2^{\bullet-}$, with stronger intensity at longer visible light exposure. Similarly, the TEMPO- h^+ peaks become moderately strong with time, indicating presence of h^+ in the medium (Fig. S4c). In contrast, the signal for TEMPO- O_2^1 was comparatively weaker which is corroborative with the results of the quenching experiments (Fig. S4d).

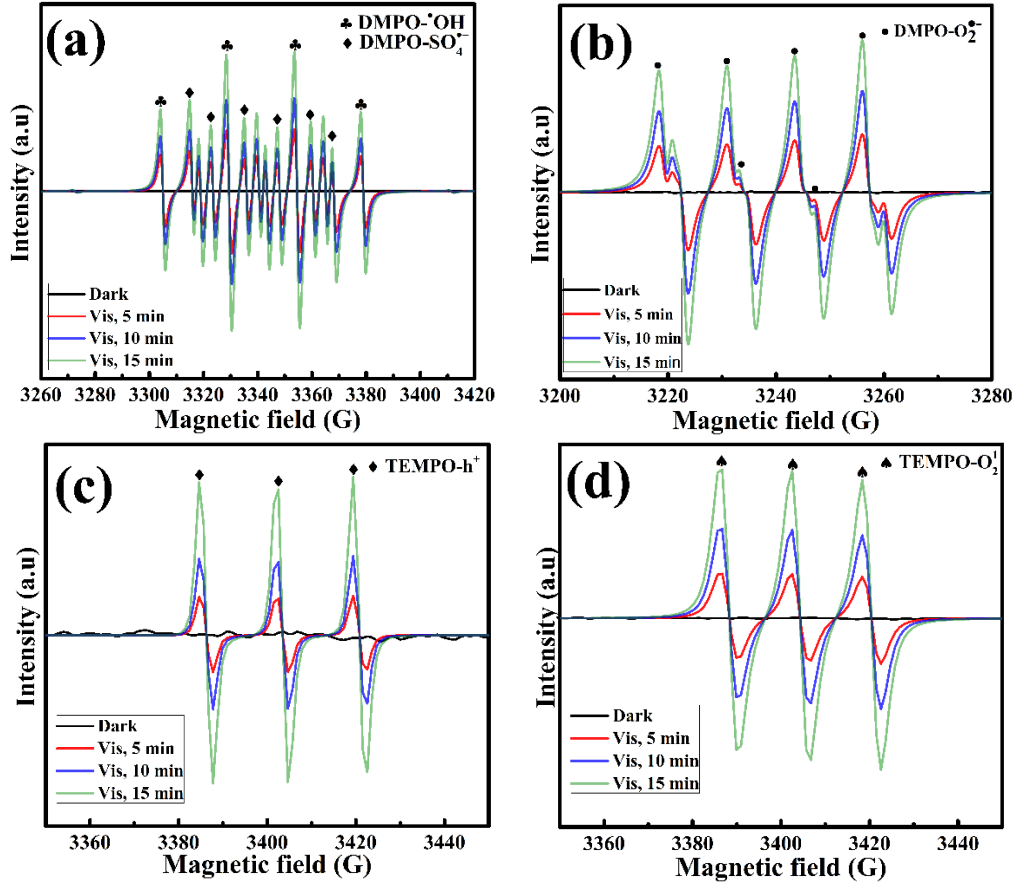
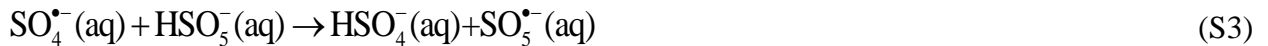


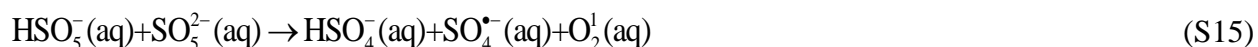
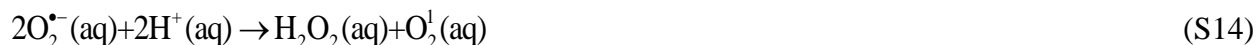
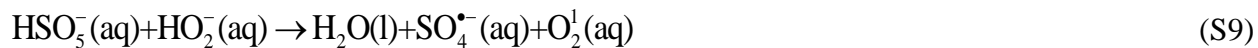
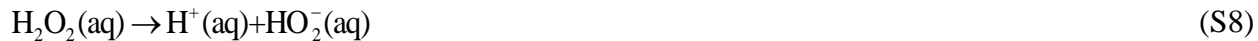
Fig. S4. EPR spectra of (a) DMPO-•OH and DMPO-SO₄^{•-}; (b) DMPO-O₂^{•-}; (c) TEMPO-h⁺; (d) TEMPO-O₂[•].

S3. The following reactions are involved in the radical quenching process at higher PMS concentrations⁵⁻⁷:

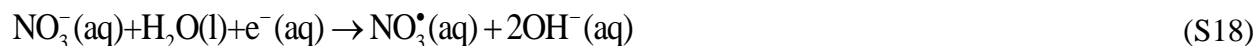


The reactions involved in the alkaline activation of PMS are given as:

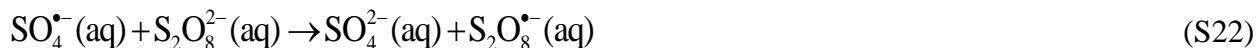
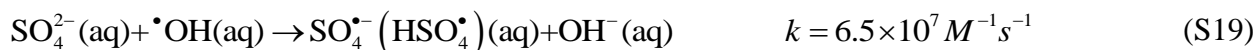




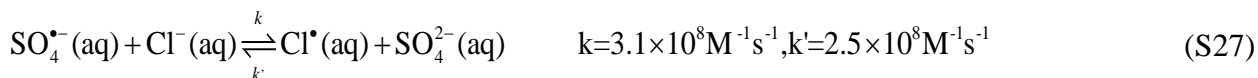
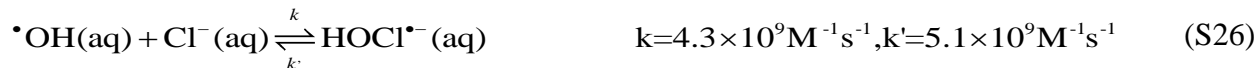
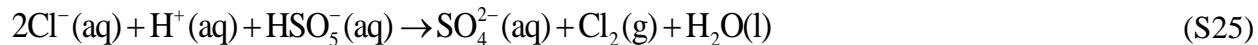
The following are the reactions that take place during the radical scavenging process by NO_3^- :



The following are the reactions that take place during the radical scavenging process by SO_4^{2-} :



The following are the reactions that take place during the radical scavenging process by Cl^- :

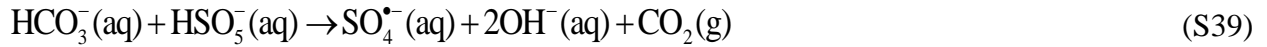
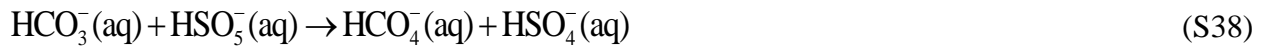
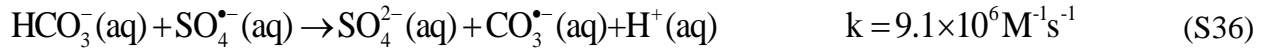




The following are the reactions that take place during the radical scavenging process by HPO_4^{2-} :



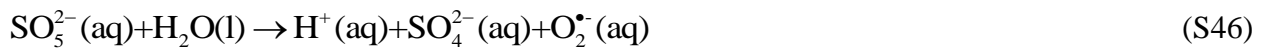
The following are the reactions that take place during the radical scavenging process by HCO_3^- :



The following are the reactions that take place during the radical scavenging process by NOM:



The following reactions are involved in the activation of PMS in presence of the binary composite catalyst:



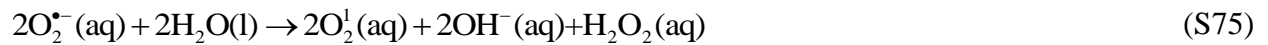
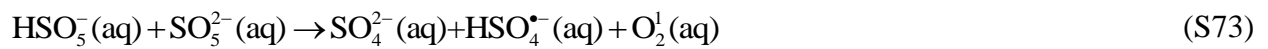
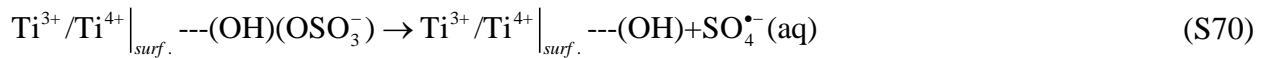
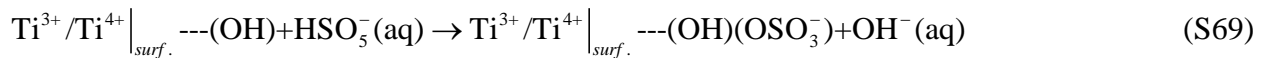
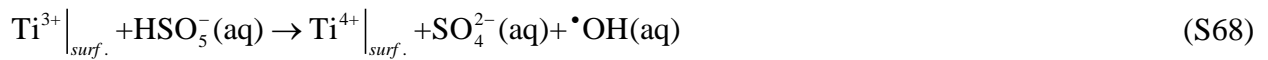
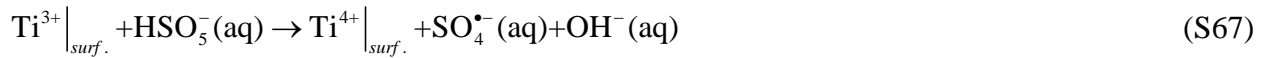
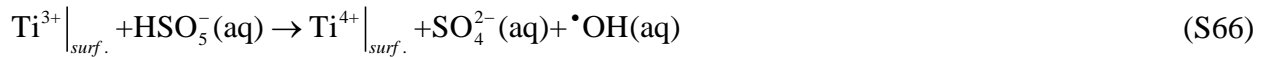
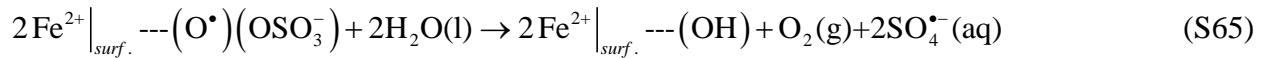
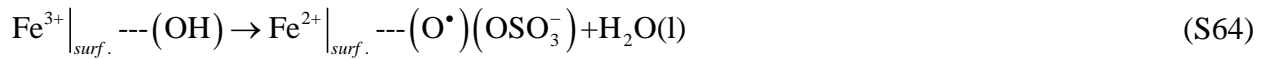
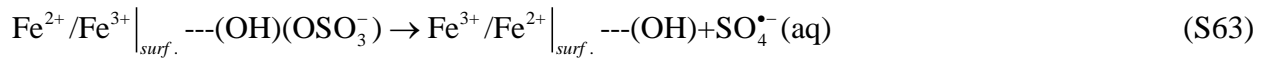
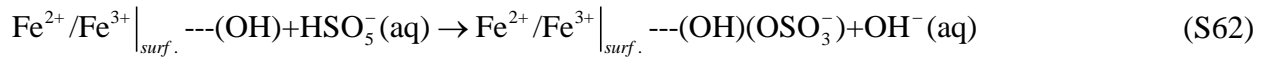
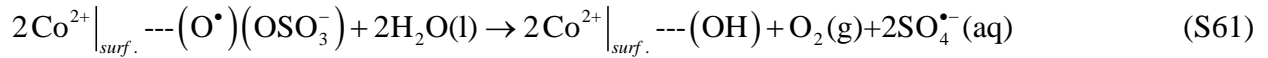
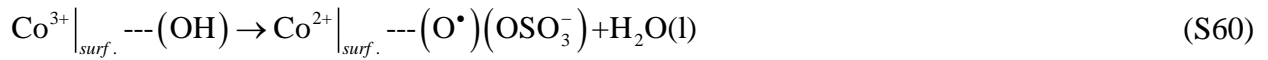
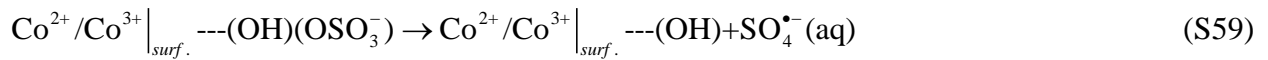
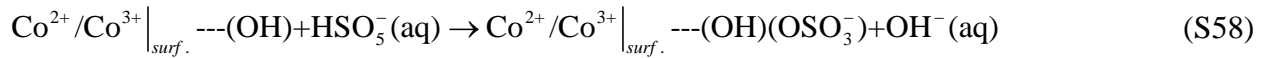
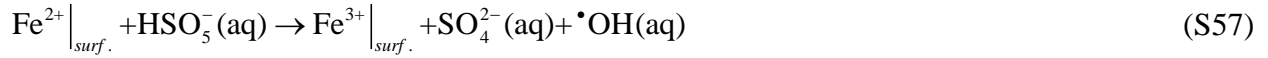
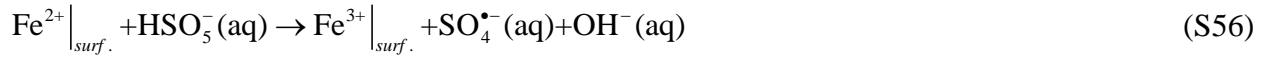
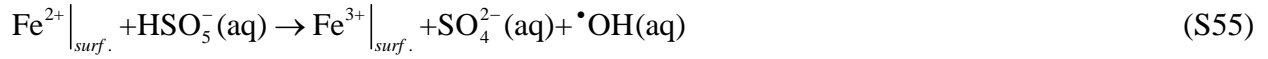
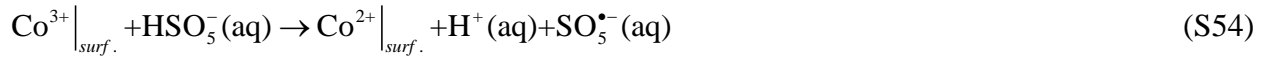
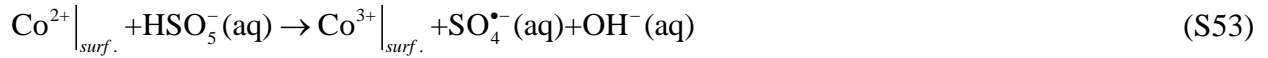
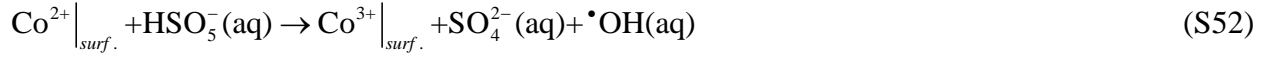
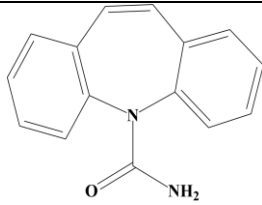
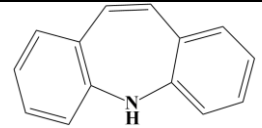
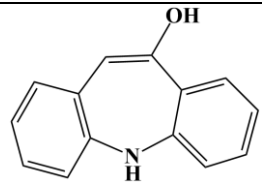
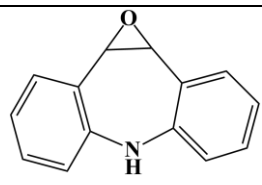
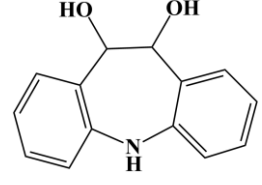
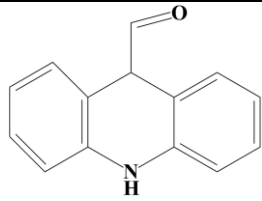
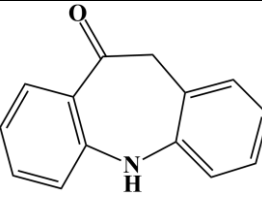
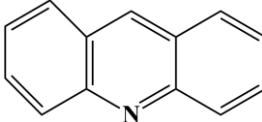
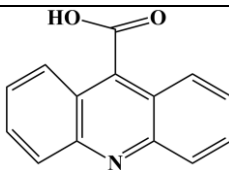
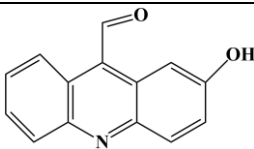
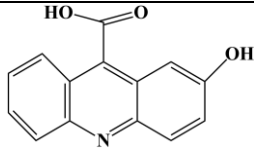
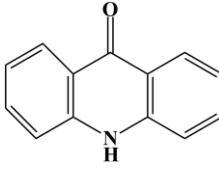
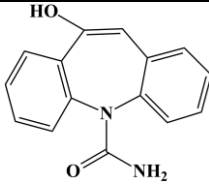


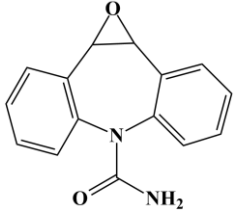
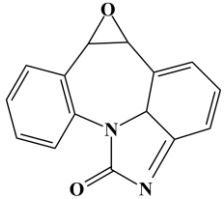
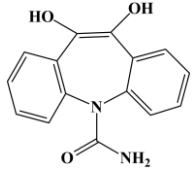
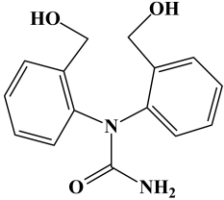
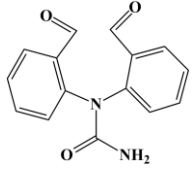
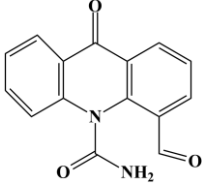
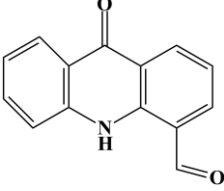
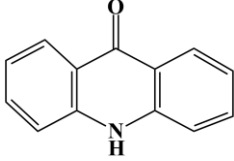
Table S1. Typical characteristics of different water matrixes

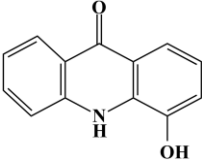
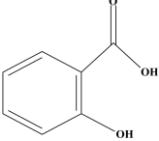
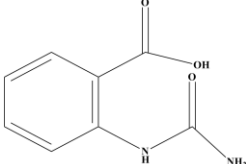
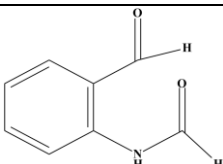
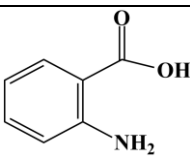
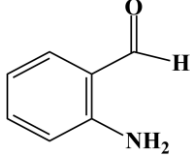
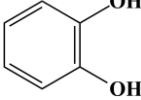
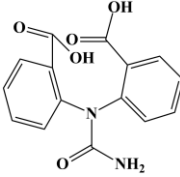
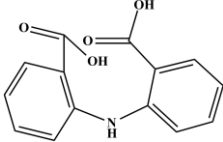
Parameters	DI water	Tap water	Lake water	River water
pH	6.7±0.8	7.7±0.5	7.4±0.5	6.8±0.5
TOC (mg/l)	-----	12.9±0.7	25.7±0.5	52.8±0.7
Chloride (Cl ⁻ , mg/l)	-----	7.3±0.8	11.5±0.3	21.7±0.3
Sulfate (SO ₄ ²⁻ , mg/l)	-----	22.2±0.5	41.8±0.8	45.7±0.3
Bicarbonate (HCO ₃ ⁻ , mg/l)	-----	15.5±0.8	37.6±0.5	47.6±0.8
Nitrate (NO ₃ ⁻ , mg/l)	-----	1.41±0.05	2.35±0.03	4.56±0.07
TDS (mg/l)	-----	107±15	245±21.8	378.8±55.2
Total Fe (mg/l)	-----	1.4±0.5	2.3±0.2	6.8±0.8

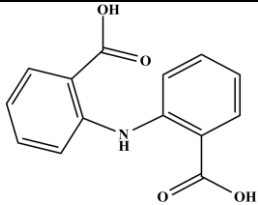
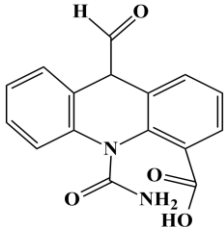
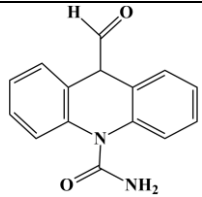
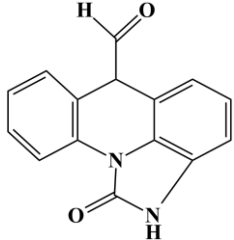
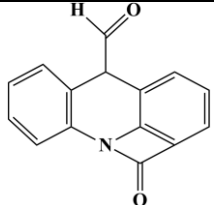
Table S2. Details of the generated intermediates from CBZ degradation

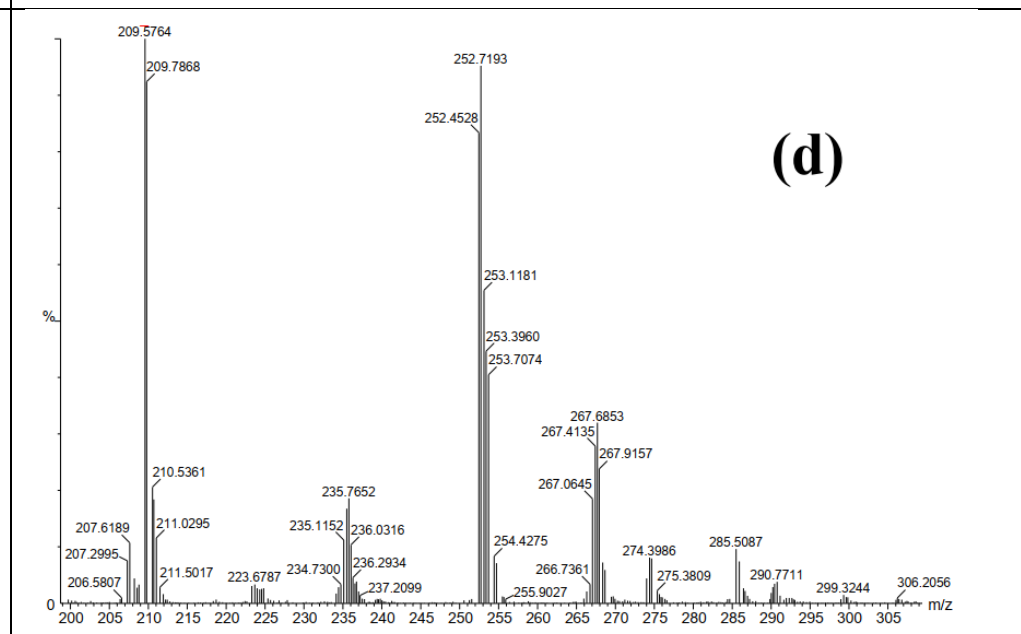
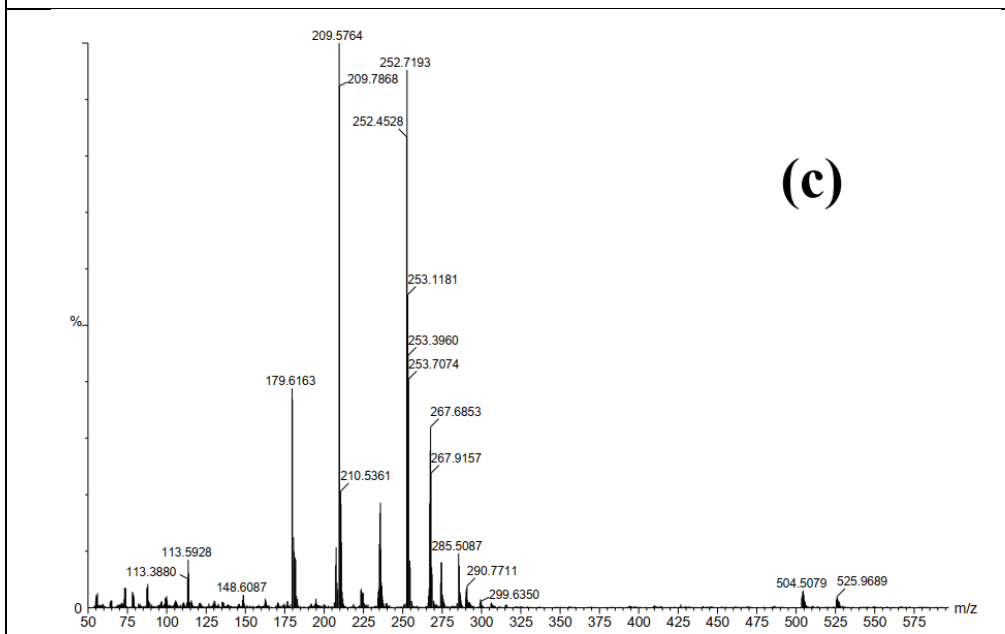
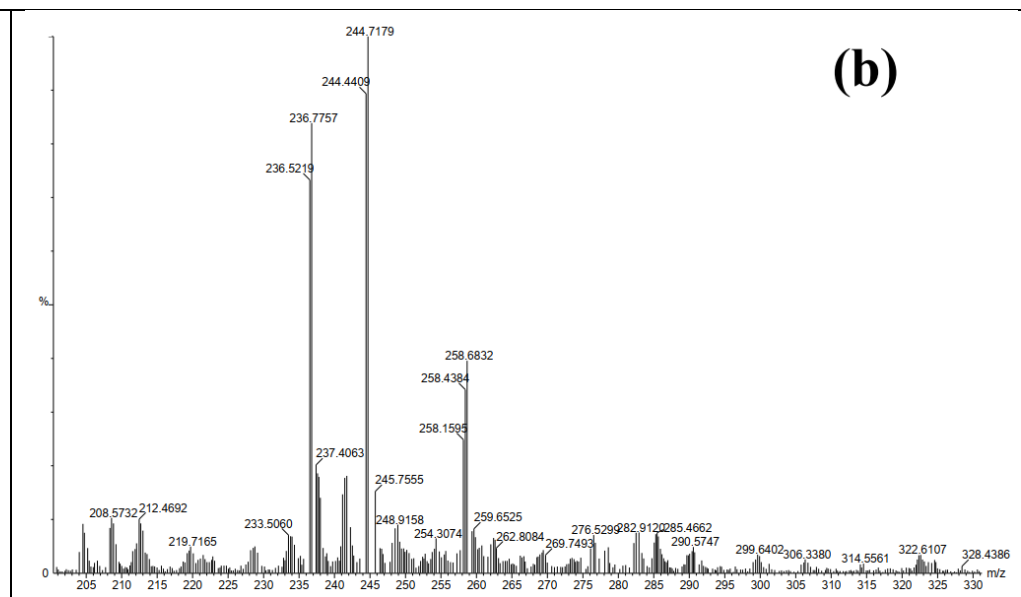
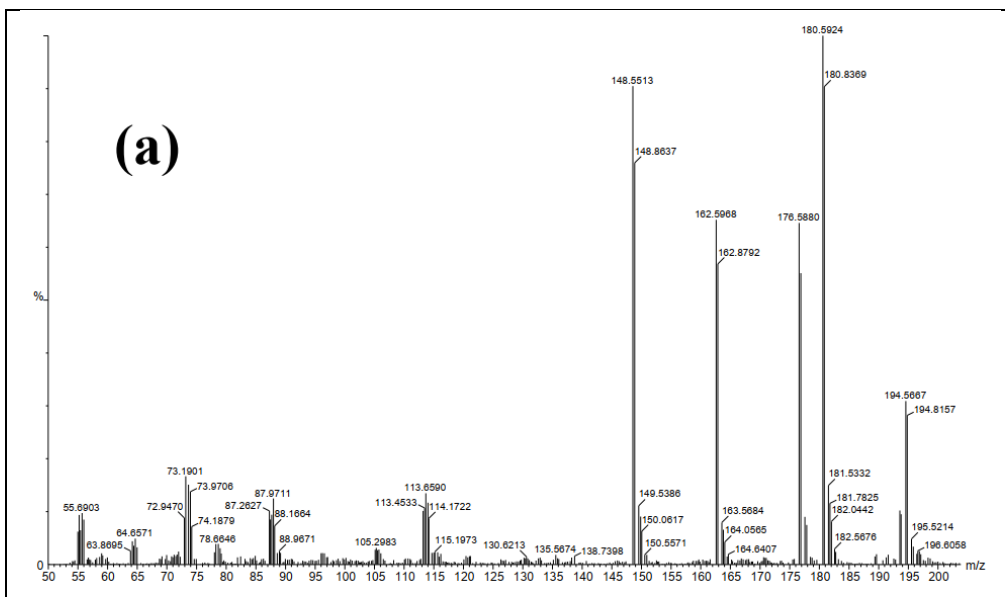
Compound	m/z	Chemical formula	Chemical Structure
Carbamazepine (CBZ)	236.27	C ₁₅ H ₁₂ N ₂ O	
P(1,1)	193.5	C ₁₄ H ₁₁ N	
P(1,2)	209.1	C ₁₄ H ₁₁ NO	
P(1,2)'	209.1	C ₁₄ H ₁₁ NO	
P(1,3)	227	C ₁₄ H ₁₃ NO ₂	

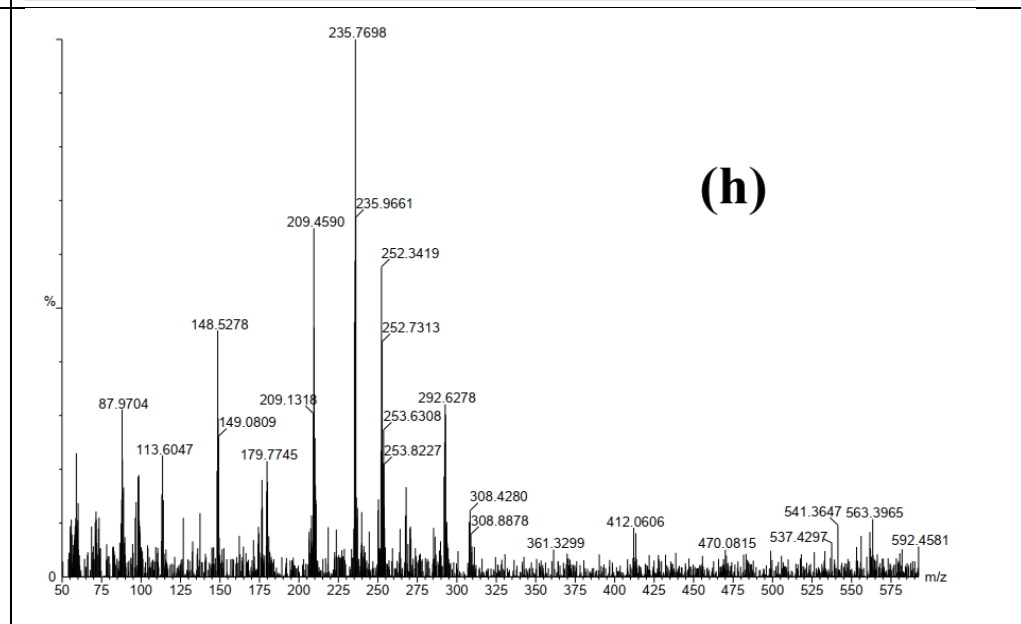
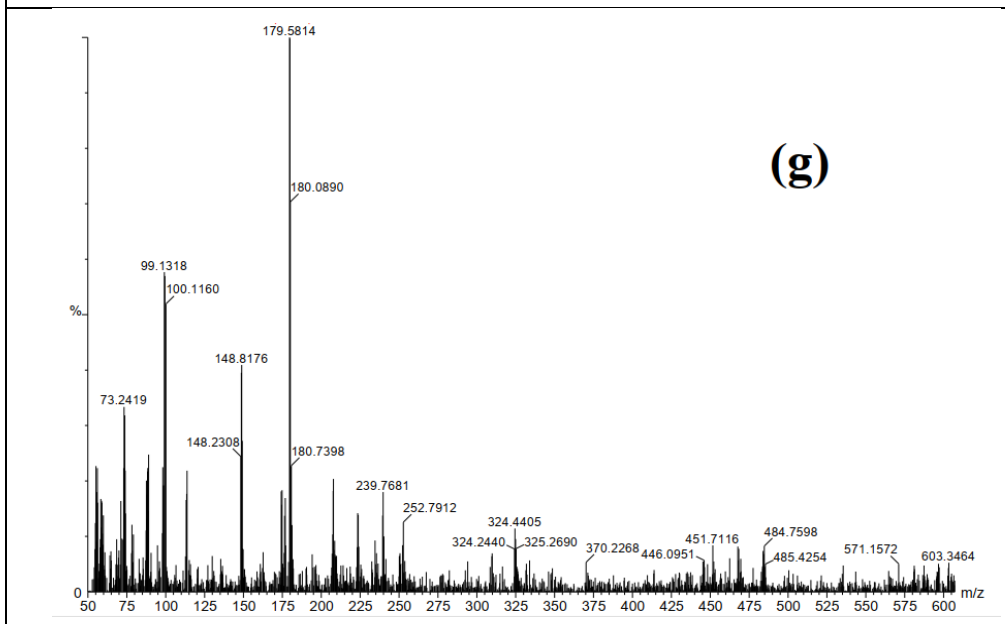
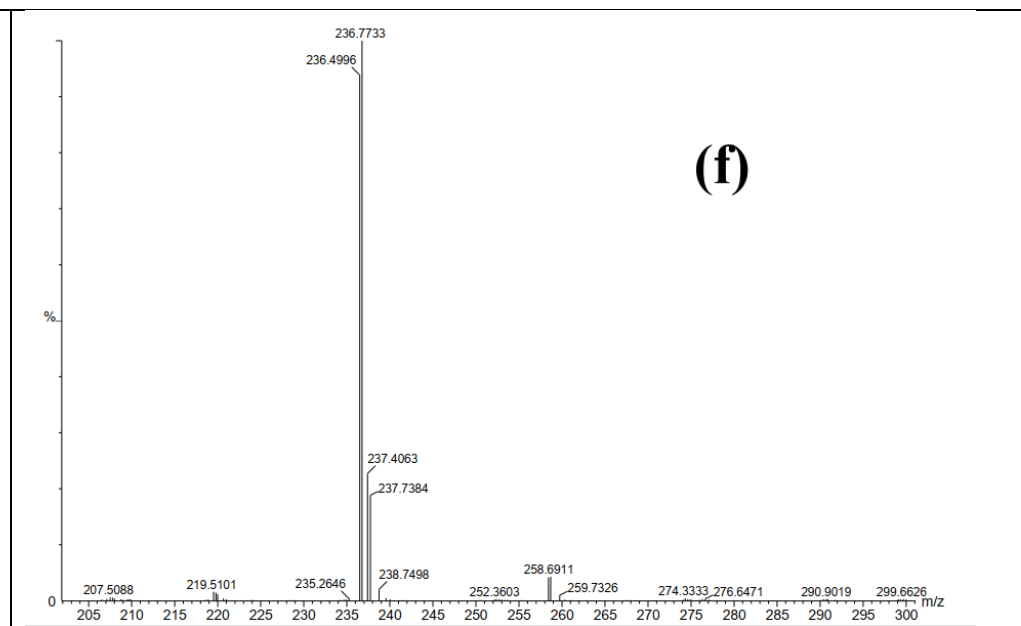
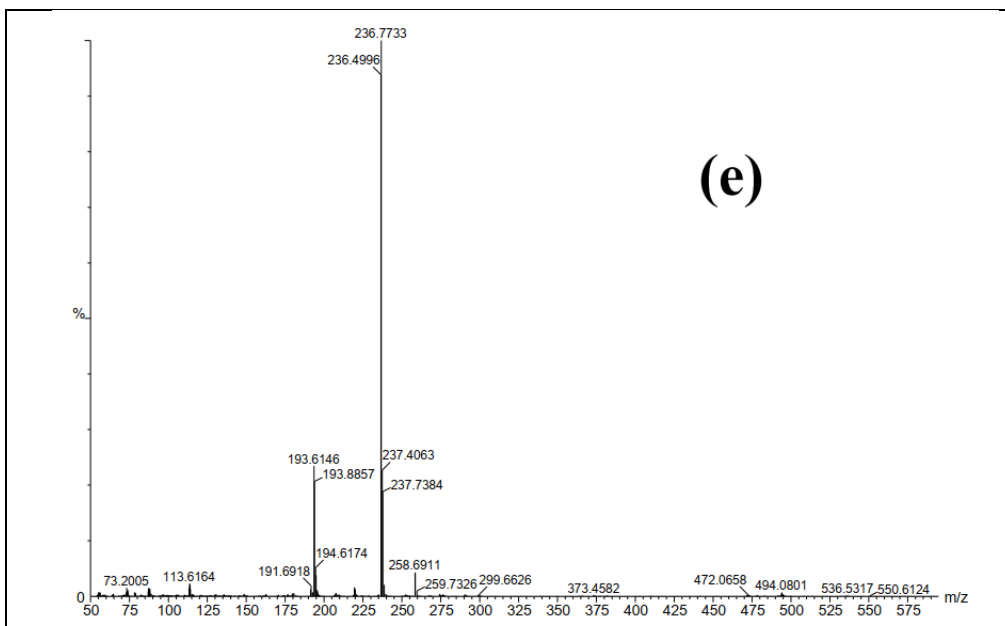
P(1,4)	209	$C_{14}H_{11}NO$	
P(1,5)	209	$C_{14}H_{11}NO$	
P(1,6)	179.1	$C_{13}H_{11}N$	
P(1,7)	223.2	$C_{14}H_9NO_2$	
P(1,8)	224.05	$C_{14}H_9NO_2$	
P(1,9)	239	$C_{14}H_9NO_3$	
P(1,10)	195.2	$C_{13}H_9NO$	
P(2,1)	252.09	$C_{15}H_{12}N_2O_2$	

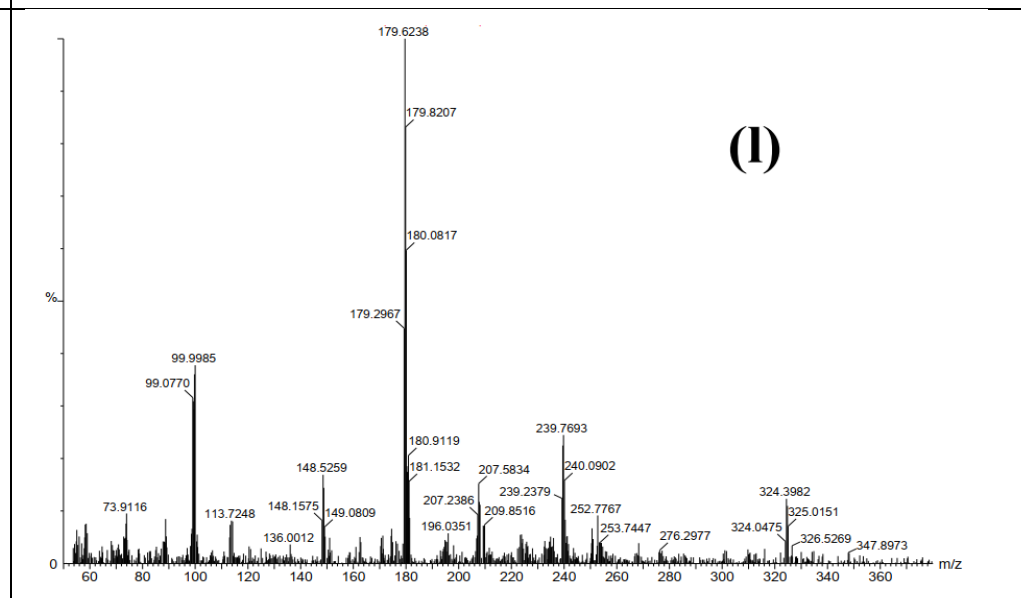
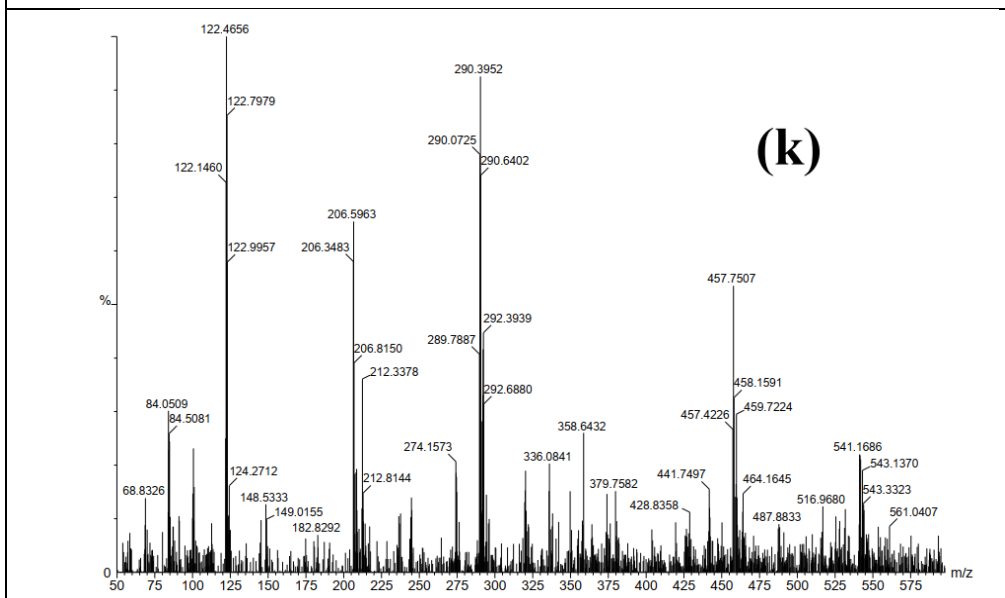
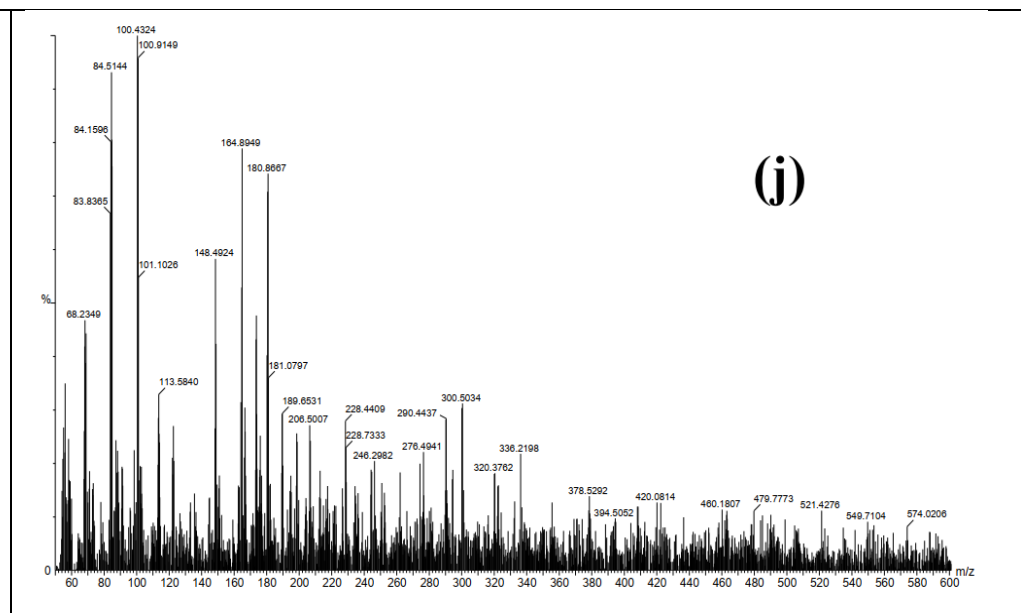
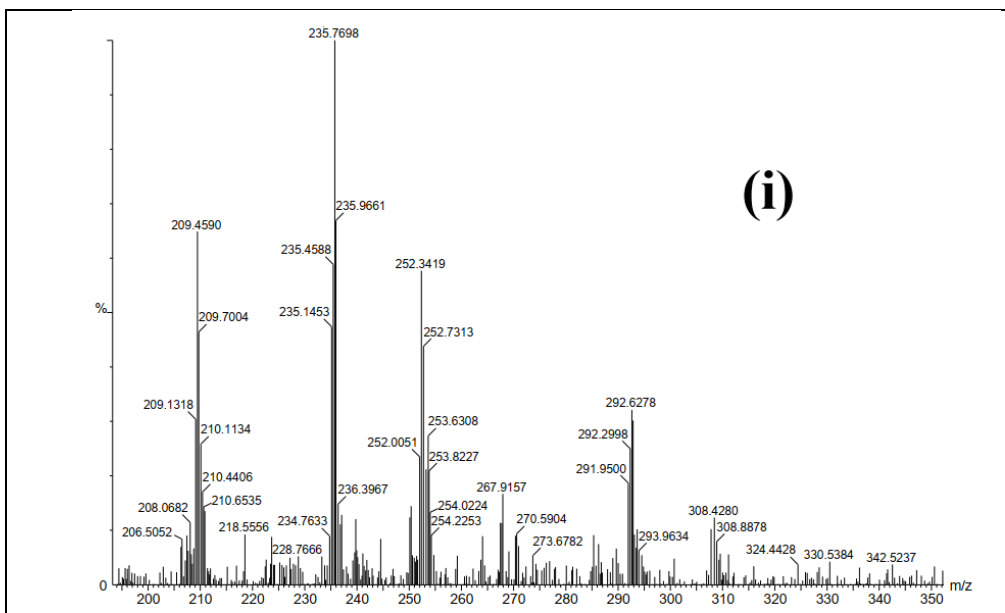
P(2,1)'	252.09	C ₁₅ H ₁₂ N ₂ O ₂	
P(2,2)	250.07	C ₁₅ H ₁₀ N ₂ O ₂	
P(3,1)	267.1	C ₁₅ H ₁₂ N ₂ O ₃	
P(3,2)	272.2	C ₁₅ H ₁₆ N ₂ O ₃	
P(3,3)	268.1	C ₁₅ H ₁₂ N ₂ O ₃	
P(3,4)	267.1	C ₁₅ H ₁₀ N ₂ O ₃	
P(3,5)	224	C ₁₄ H ₉ NO ₂	
P(3,6)	195.1	C ₁₃ H ₉ NO	

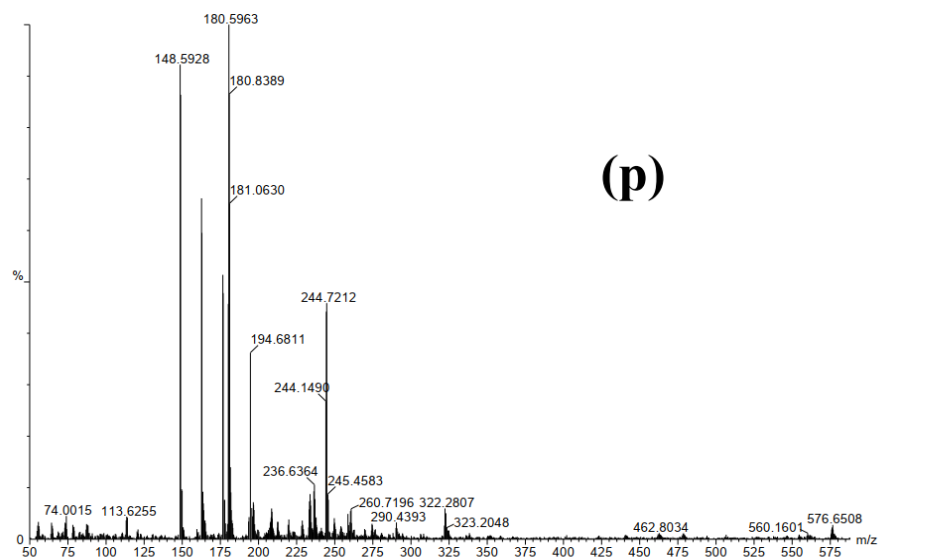
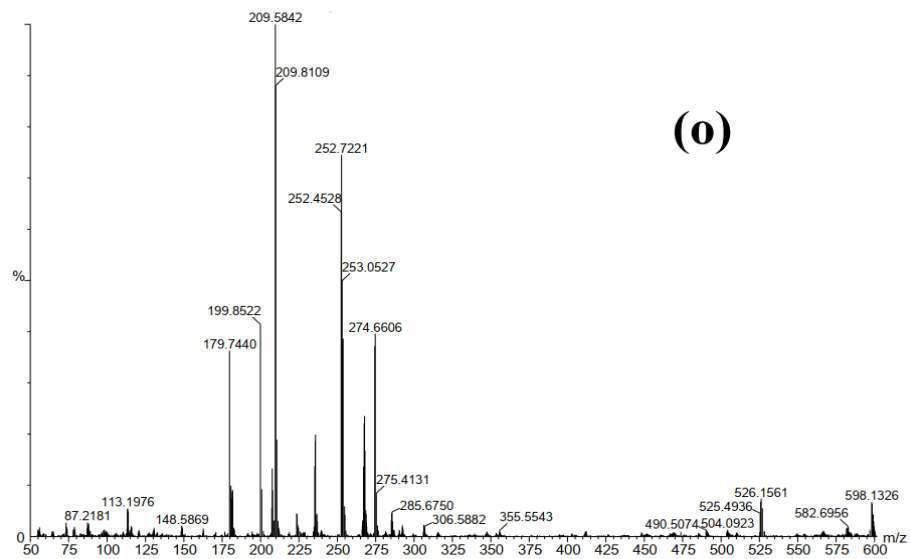
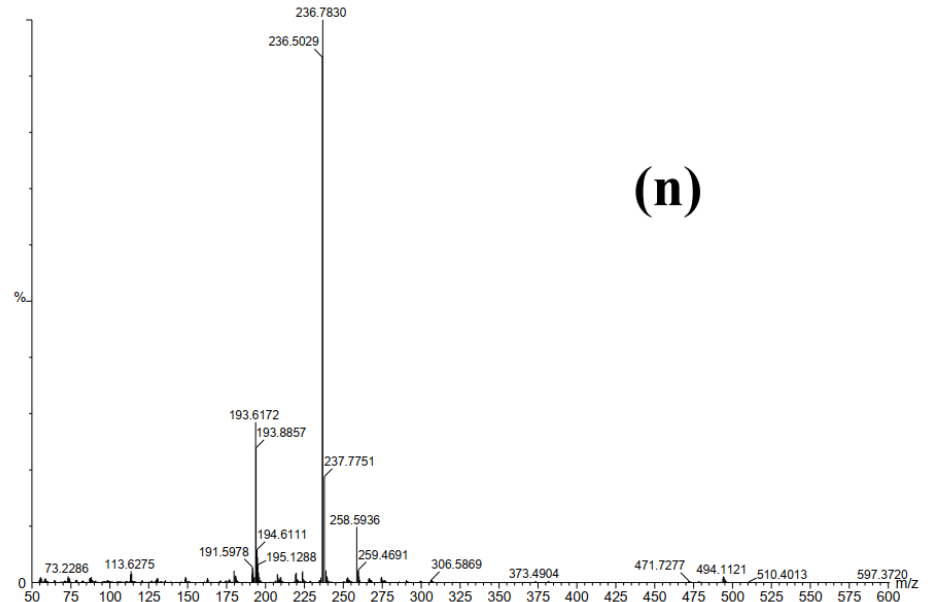
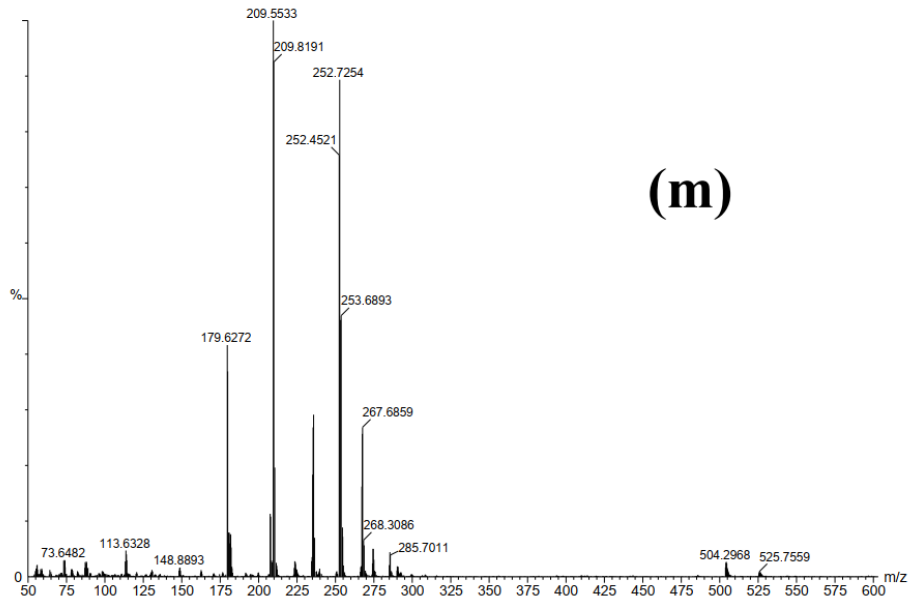
P(3,7)	211.1	$C_{13}H_9NO_2$	
P(3,8)	138.03	$C_7H_6O_3$	
P(3,9)	181	$C_8H_8N_2O_3$	
P(3,10)	149	$C_8H_7NO_2$	
P(3,11)	137.1	$C_7H_7NO_2$	
P(3,12)	121	C_7H_7NO	
P(3,13)	110	$C_6H_6O_2$	
P(4,1)	300.07	$C_{15}H_{12}N_2O_5$	
P(4,2)	257.07	$C_{14}H_{11}NO_4$	

P(4,2)'	257.07	$C_{14}H_{11}NO_4$	 <p>The structure shows a benzimidazole ring system. One nitrogen atom is bonded to a phenyl ring, and the other is bonded to a benzene ring that has a hydroxyl group (-OH) and a carboxylic acid group (-COOH) attached to it.</p>
P(4,3)	296.05	$C_{16}H_{12}N_2O_4$	 <p>The structure features a benzimidazole core. One nitrogen is bonded to a phenyl ring, and the other is bonded to a benzene ring with a hydroxyl group (-OH) and a carboxamide group (-CONH₂) attached. Additionally, a formyl group (-CHO) is attached to the carbon atom between the two nitrogens.</p>
P(4,4)	252.09	$C_{15}H_{12}N_2O_2$	 <p>The structure shows a benzimidazole core. One nitrogen is bonded to a phenyl ring, and the other is bonded to a benzene ring with a carboxamide group (-CONH₂) attached. A formyl group (-CHO) is attached to the carbon atom between the two nitrogens.</p>
P(4,5)	250.07	$C_{15}H_{10}N_2O_2$	 <p>The structure features a benzimidazole core. One nitrogen is bonded to a phenyl ring, and the other is bonded to a benzene ring with a formyl group (-CHO) attached. The carbon atom between the two nitrogens is also bonded to a formyl group (-CHO).</p>
P(4,6)	235.06	$C_{15}H_9NO_2$	 <p>The structure shows a benzimidazole core. One nitrogen is bonded to a phenyl ring, and the other is bonded to a benzene ring with a carbonyl group (=O) attached. A formyl group (-CHO) is attached to the carbon atom between the two nitrogens.</p>









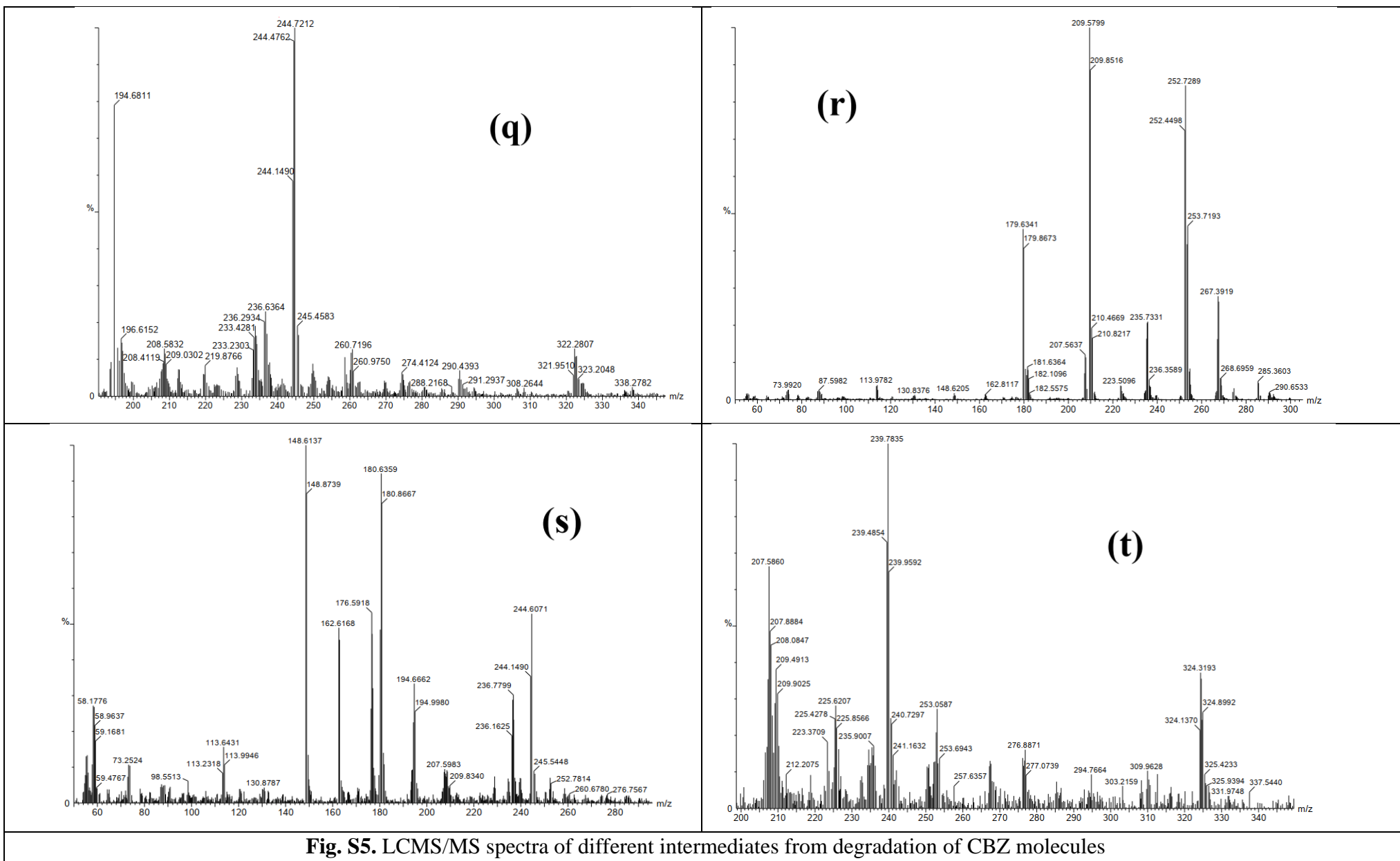


Fig. S5. LCMS/MS spectra of different intermediates from degradation of CBZ molecules

Table S3: Comparative analysis of the catalytic activity of different materials

Sl. No	Catalyst	Catalyst dose (g/L)	PMS dose (g/L)	CBZ concentration (mg/L)	Temperature (°C)	pH	Reaction time (min)	Degradation extent (%)	Synthesis method of catalyst	Reaction rate constant (min ⁻¹)	References
1	MoS ₂	0.2	0.03	5	30	5.8	40	> 95%	Hydrothermal method	0.0861	⁸
2	N-CFA	0.2	0.6	10	25	5	50	100%	Carbonization in N ₂ atmosphere	0.092	⁹
3	Co-RH-130	0.2	0.3	20	25	6.9	60	95.78%	Hydrothermal method	0.0764	¹⁰
4	CuFe ₂ O ₄	0.1	0.2	10	25	6.5	120	90%	Hydrothermal and annealing	0.029	¹¹
5	FeS ₂ and WS ₂ mixture	0.1(FeS ₂), 0.15(WS ₂)	0.03	2	30	6.7	40	99%	Commercial	0.108	¹²
6	CoFe ₂ O ₄ /rGO	0.2	0.14	50	n/a	6.5 2	30	93.19%	Solvothermal method	0.11	¹³
7	AMIL(10)@MIL	0.05	0.25	10	30	6.5	60	99.9%	Hydrothermal method	0.089	Present study

S3. References

- 1 M. Xie, Y. Ma, D. Lin, C. Xu, F. Xie and W. Zeng, Bimetal–organic framework MIL-53(Co–Fe): an efficient and robust electrocatalyst for the oxygen evolution reaction, *Nanoscale*, 2020, **12**, 67–71.
- 2 X. Yang, W. Gu, Y. Ma, S. Zhai and F. Teng, Interface electron transfer of Bi₂MoO₆/MIL-125 and the visible-light performance for pollutant degradation, *Colloids Surfaces A Physicochem. Eng. Asp.*, 2020, **597**, 124748.
- 3 S. Zhang, M. Du, J. Kuang, Z. Xing, Z. Li, K. Pan, Q. Zhu and W. Zhou, Surface-defect-rich mesoporous NH₂-MIL-125 (Ti)@Bi₂MoO₆ core-shell heterojunction with improved charge separation and enhanced visible-light-driven photocatalytic performance, *J. Colloid Interface Sci.*, 2019, **554**, 324–334.
- 4 M. Govarthanan, R. Mythili, W. Kim, S. Alfarraj and S. A. Alharbi, Facile fabrication of (2D/2D) MoS₂@MIL-88(Fe) interface-driven catalyst for efficient degradation of organic pollutants under visible light irradiation, *J. Hazard. Mater.*, 2021, **414**, 125522.
- 5 P. Sarkar, D. Roy, B. Bera, S. De and S. Neogi, Efficient photocatalytic degradation of ciprofloxacin using novel dual Z-scheme gCN/CuFe₂O₄/MoS₂ mediated peroxymonosulphate activation, *Chem. Eng. J.*, 2022, **430**, 132834.
- 6 D. Roy, S. Neogi and S. De, Mechanistic investigation of photocatalytic degradation of Bisphenol-A using MIL-88A(Fe)/MoS₂ Z-scheme heterojunction composite assisted peroxymonosulfate activation, *Chem. Eng. J.*, 2022, **428**, 131028.
- 7 D. Roy, S. Neogi and S. De, Visible light assisted activation of peroxymonosulfate by bimetallic MOF based heterojunction MIL-53(Fe/Co)/CeO₂ for atrazine degradation: Pivotal roles of dual redox cycle for reactive species generation, *Chem. Eng. J.*, 2022, **430**, 133069.
- 8 H. Zhou, L. Lai, Y. Wan, Y. He, G. Yao and B. Lai, Molybdenum disulfide (MoS₂): A versatile activator of both peroxymonosulfate and persulfate for the degradation of carbamazepine, *Chem. Eng. J.*, 2020, **384**, 123264.
- 9 S. Liu, C. Zhao, Z. Wang, H. Ding, H. Deng, G. Yang, J. Li and H. Zheng, Urea-assisted one-step fabrication of a novel nitrogen-doped carbon fiber aerogel from cotton as metal-free catalyst in peroxymonosulfate activation for efficient degradation of carbamazepine, *Chem. Eng. J.*, 2020, **386**, 124015.
- 10 Y. Li, S. Zhang, Y. Qin, C. Yao, Q. An, Z. Xiao and S. Zhai, Preparation of cobalt/hydrochar using the intrinsic features of rice hulls for dynamic carbamazepine degradation via efficient PMS activation, *J. Environ. Chem. Eng.*, 2022, **10**, 108659.
- 11 S.-F. Jiang, L. Wang, W.-F. Hu, K. Tian and H. Jiang, Preparation of Flower-like CuFe₂O₄ by a Self-Templating Method for High-Efficient Activation of Peroxymonosulfate To Degrade Carbamazepine, *Ind. Eng. Chem. Res.*, 2021, **60**, 11045–11055.
- 12 G. Gou, S. Kang, H. Zhao, C. Liu, N. Li, B. Lai and J. Li, Efficient peroxymonosulfate activation through a simple physical mixture of FeS₂ and WS₂ for carbamazepine

degradation, *Sep. Purif. Technol.*, 2022, **290**, 120828.

- 13 Y. Zhang, Y. Cheng and H. Qi, Synergistic degradation of organic pollutants on CoFe₂O₄/rGO nanocomposites by peroxydisulfate activation under LED irradiation, *Appl. Surf. Sci.*, 2022, **579**, 152151.